



The impact of utilizing ultra-high performance fiber-reinforced concrete in beam-column joints with different patterns of transverse reinforcement

Ayman Abdo, Heba A. Mohamed, Talaat Ryad, Sayed Ahmed

University of Zagazig, Egypt

eng_a_abdo@yahoo.com, <http://orcid.org/0000-0003-4040-6032>

hebanahbe@yahoo.com, talaat.reyadfatehy@gmail.com

sayedahmed.str@gmail.com, <http://orcid.org/0000-0002-8272-5114>



ABSTRACT. This research studies and assesses the possibility of employing ultra-high performance fiber reinforced concrete (UHPFRC) in exterior beam-column joints (BCJs). Eight specimens with various concrete material characteristics and steel reinforcing details are cast and examined under repeated loads. Normal concrete with seismic reinforcing details is used as a control specimen. For certain specimens, UHPC, UHPFRC with 1% steel fiber, and UHPFRC with 2% steel fiber are poured into all BCJs, and others are poured into the critical zone only. The consequences of removing stirrups from the joint were studied. All specimens' crack patterns, hysteresis and envelope curves, ductility factor, stiffness degradation, and energy dissipation are assessed and corresponded to the control sample. The results demonstrate that UHPFRC strengthened the joint, prevented crack development and extension and the shear failure in the joint, and formed the plastic hinge in the beams. UHPFRC outperforms normal concrete with seismic reinforcing details and UHPC without steel fiber in bearing capacity, ductility, stiffness, and energy dissipation. UHPFRC with 1% steel fiber enhanced joint behavior, while UHPFRC with 2% steel fiber was better. Casting the whole sample with UHPFRC achieved very little improvement. The presence of stirrups in the UHPFRC beam-column joint has little effect on its properties. It is more economical to cast UHPFRC in the joint zone only and reduce or eliminate these stirrups in the case of UHPFRC.

KEYWORDS. UHPFRC, BCJ, Repeated loading, Shear reinforcement, Crack pattern.

Citation: Abdo, A., Mohamed, H. A., Ryad, T., Ahmed, S., The impact of utilizing ultra-high performance fiber-reinforced concrete in beam-column joints with different patterns of transverse reinforcement, *Frattura ed Integrità Strutturale*, 64 (2023) 11-30.

Received: 16.11.2022

Accepted: 12.01.2023

Online first: 14.01.2023

Published: 01.04.2023

Copyright: © 2023 This is an open access article under the terms of the CC-BY 4.0, which permits unrestricted use, distribution, and reproduction in any medium, provided the original author and source are credited.

INTRODUCTION

The beam-column joints (BCJs) are the most susceptible sections of all constructions, resulting in a massive failure. The exterior BCJs are more susceptible than the interior joints because beams constrain the inside joints, but the external joints aren't. As a result, the researchers were interested in repairing external reinforced concrete (RC) beam-to-column connections in buildings. Researchers employed various strengthening materials and techniques to improve the brittle susceptible junctions' ductility and load-bearing capabilities [1]. The pattern of BCJ damage in buildings subjected to the October 1992 earthquake in Egypt revealed that inadequate shear reinforcement of the joint, particularly the exterior one, was one of the principal sources of joint damage. More attention should be given to the design of the joint area, as most of the codes consider the joint area to be rigid. However, some research emphasized the importance of considering the joint area as flexible and ductile [2,3].

The strut and truss mechanisms are two methods to resist shear force acting on the joints [4]. The only factor on which the strut mechanism relies is the concrete of the joint core. The shear force exerted at the joint core's perimeter by the bond force between the longitudinal bars and the concrete makes the truss mechanism work. Seismic behavior can be improved by increasing the ductility of the joints and ensuring that the failure occurs in the beam and not in the joint [5,6]. Beam flexural yielding, joint shear failure, beam flexural failure without joint failure, and column flexure yielding are all joint failures [7]. Increasing the ratio between joint shear capacity and joint shear demand evaluated according to the beam yield and hardening mechanism makes the failure tends to be flexural in the beam [8]. The shear stress produced in the joint must not exceed the joint shear strength to conform to the capacity design philosophy [9]. Joints must resist seismic forces until the adjoining members reach their inelastic deformations. The shear strength of joints is affected by the compressive strength of concrete. Most design regulations regard the square root of the concrete compressive strength as a factor of joint shear capacity. Compressive strength is the most effective parameter for resisting shear stress. The bearing stress between steel bars and concrete increases by increasing the concrete compressive strength [10-11]. The use of stirrups in the joint limits the concrete in the core and creates a diagonal compression field in the joint zone, which helps resist shear strength [12]. The shear strength of joints increases as the stirrups ratio increases [12]. Joint shear strength is affected by depth aspect ratios [13]; proper anchoring to longitudinal beam bars in a joint prevents beam bars from pulling out, increases bond strength, and influences joint shear strength [14-16]. In old structures, the degree of steel reinforcement corrosion and the corrosion rate affect the joints' mechanical performance [17].

Ultra-high performance concrete (UHPC) contains a high cement content, small aggregate size, binder (fly ash, silica fume), and 0.2 water-cement ratios (the water/cement ratio in the concrete mix is the amount of water per amount of cement by weight) to avoid the formation of air voids in the mix. Curing regimes influence the mechanical behavior of UHPC, especially compressive strength. Compared to traditional concrete, combining the above ingredients in certain proportions can improve concrete performance, greater durability, and increased bearing capacity. Fiber addition substantially enhances the tensile capacity before fracture localization and strength depletion. UHPFRC has a compressive strength of up to 150 MPa and tensile strength of 6.2 MPa [18]. Using UHPFRC in flexure members like beams and compression members like columns was suggested in many studies [19-24].

Yuan et al. [25] tested BCJs under reversed cyclic loading to study the effect of replacing concrete with engineered cementitious composite (ECC) in the joint zone on the seismic behavior of members. The results assured that samples with ECC and without shear reinforcement can't change brittle failure mode but can increase the load capacity, ductility, and energy dissipation. BCJs were tested under monotonic and cyclic loading and replaced the joint region concrete with UHPC and UHPFRC [26]. The results showed that thrived-carrying capacity and joint shear strength were improved in hybrid samples, and the joint shear failure changed to beam flexural failure. Because of the beam's flexural failure, it was impossible to examine the impact of the ties on the steel fiber reinforced concrete (SFRC) and UHPC joint areas. Zheng et al. [27] investigated the seismic behavior of reactive powder concrete (RPC) (a type of UHPFRC) for interior BCJs subjected to cyclic loading. The results showed that joints with RPC have a higher crack resistance, shear carrying capacity, and strength. Additionally, using RPC in joints reduces joint stirrups. Shear force in the RPC joint depends mainly on the diagonal strut mechanism. The application of engineered cementitious composite in BCJs required more studies [28-29].

Sarmiento et al. [30] carried many cyclic loads on UHPFRC-BCJ specimens. The results assured that UHPFRC specimens dissipate energy more than non-fiber normal RC specimens. Fudong et al. [31] studied five precast BCJs connected with lap-spliced steel bars in UHPC. The results showed that UHPC enhanced the joints' shear capacity due to high shear strength and increased the ductility of the joints. Abusafaqa et al. [32] constructed a parametric study on exterior BCJ with UHPC. Compared to a unique moment-resistant frame, the findings demonstrate that UHPC-strengthened joints can independently achieve the necessary degree of ductility and strength.



Researchers have not thoroughly investigated the UHPFRC effect on the performance of exterior BCJs under cyclic loads. The behavior of UHPFRC-BCJs with different steel fibers volume fraction ratios, various shear reinforcement details, and using normal concrete (NC) and UHPFRC in the same joint have not been investigated sufficiently. Consequently, this study investigates the impact of utilizing UHPFRC materials in exterior BCJs with different steel fibers volume fraction ratios and shear reinforcement details. The crack patterns and mode failure, hysteresis and envelope behavior, ductility index, stiffness degradation, and energy dissipation were investigated in detail. In this research, the effect of different types of concrete (NC, UHPC, and UHPFRC) on the behavior of the beam-column joint will be studied. The effect of using end-hooked steel fibers with 1 and 2% on the behavior of the joint will be studied. The effect of casting UHPFRC in the whole specimen or the critical joint zone only will be studied. The effect of condensing stirrups at the joint critical zone will be studied. The effect of eliminating the stirrups from the joint zone will be studied.

EXPERIMENTAL WORK

Material characteristics

The four mixes used in this study are normal concrete mix (NC), ultra-high performance concrete (UHPC), ultra-high performance fiber reinforced concrete UHPFRC1 with 1% steel fiber, and ultra-high performance fiber reinforced concrete UHPFRC2 with 2% steel fiber.

Normal concrete mix

The normal concrete mix consists of Ordinary Portland Cement (OPC) with high-grade 52.5N, natural crushed available coarse aggregates with specific gravity (SG) = 2.64 and maximum nominal size = 20mm, clean siliceous sand with SG = 2.69, and clean tap drinking water free from impurities [water/cement ratio (w/c) = 0.4]. The concrete mixer was used to cast the concrete. The mixing procedure was carried out at room temperature (25 °C) according to ECP 203-2018 [33]. Because it is critical to have a homogenous concrete mix, the dry ingredients (dolomite, cement, and sand) were first weighed and mixed in the mixer for about one minute before adding 50 percent of the required water and cement. Then the remaining 50% of the needed water was added. After that, the materials were mechanically combined for around 5 minutes. At the time of testing, the hardened concrete properties were determined using standard cylinder tests (150 x 300 mm) and standard cube tests (100 x 100 x 100 mm).

UHPC and UHPFRC mix

OPC, Silica fume, Silica Sand, Steel fiber, super-plasticizer (SP), and water are used in UHPC mixtures. Silica fume (Sika Fume®-HR) was used as a secondary reactive binder to replace cement. Sika Fume®-HR contains extremely fine (0.1 μm) latently reactive silicon dioxide. This chemical improves internal cohesiveness and water retention significantly. The concrete becomes exceedingly soft, and the pumping qualities increase significantly. In the set concrete, the latently reactive silica fume forms a chemical bond with the free lime [34]. Silica sand of size 0.5 mm. The shape and geometry of steel fibers are shown in Fig. 1 [length/diameter of steel fiber (L/D) = 50]. The super-plasticizer (Sika® ViscoCrete® 2100) was added to achieve the desired workability [34]. Finally, clean drinking water is free from impurities (w/c ratio = 0.18).

The modified Andreasen and Andersen model was used to design the concrete mix to get the maximum packing density of the mix. The modified Andreasen and Andersen Eqn. (1) was used to draw the target curve of the mix and then compare it with the composition curve drawn depending on the assumed proportions of the materials. Tab. 1 shows the weight (Kg) of every component per m³ of the mix. Fig. 2 shows the grading curve of the used materials, target, and final composition curve.

$$P(D) = \frac{D^q - D_{\min.}^q}{D_{\max.}^q - D_{\min.}^q} * 100 \quad (1)$$

Note: D = particle size, μm; D_{min.} = Minimum particle size, μm; D_{max.} = maximum particle size, μm; P (D) = fraction of the total solids being smaller than size D; q = distribution modulus (0.23).

The casting of UHPC and UHPFRC mixes

The concrete mixer was used to cast the mixes. The following steps were done to produce the mix: a) all powders and sand were weighed and then poured into a mixer for dry mixing (120 s at low speed). b) Around 75% water is added and mixed

for 120 s (low speed). The mixer is stopped for 30 s after. c) the remaining water and SP are added, then the mixer works at low speed for 180 s. d) the mixture is at a high mixing speed for 120 s. Samples were well covered with burlap that was submerged in water before. Samples were sprinkled twice with water every day for 28 days. Compression test on cubes (100*100*100 mm) for different types of concrete was performed at ages 7 and 28 days of curing in water. The compressive properties of materials have been set according to the ASTM C39/C39M-10 standard. Tab. 2 shows the compressive strength of different types of used concrete.



Figure 1: Hooked-end steel fiber. a) steel fiber set, b) fiber Dimension.

	Cement	Silica fume	Sand 0-0.5mm	Sand 0-2 mm	Super-plasticizer	Water	Fine aggregate	Coarse aggregate	Steel fiber (%)
NC	450	-	-	-	-	180	548	1279	0
UHPC	884	41	227.5	1090	45.5	170	0	0	0
UHPFRC1	884	41	227.5	1065	45.5	170	0	0	1
UHPFRC2	884	41	227.5	1045	45.5	170	0	0	2

Table 1: Mix proportion (kg/m³)

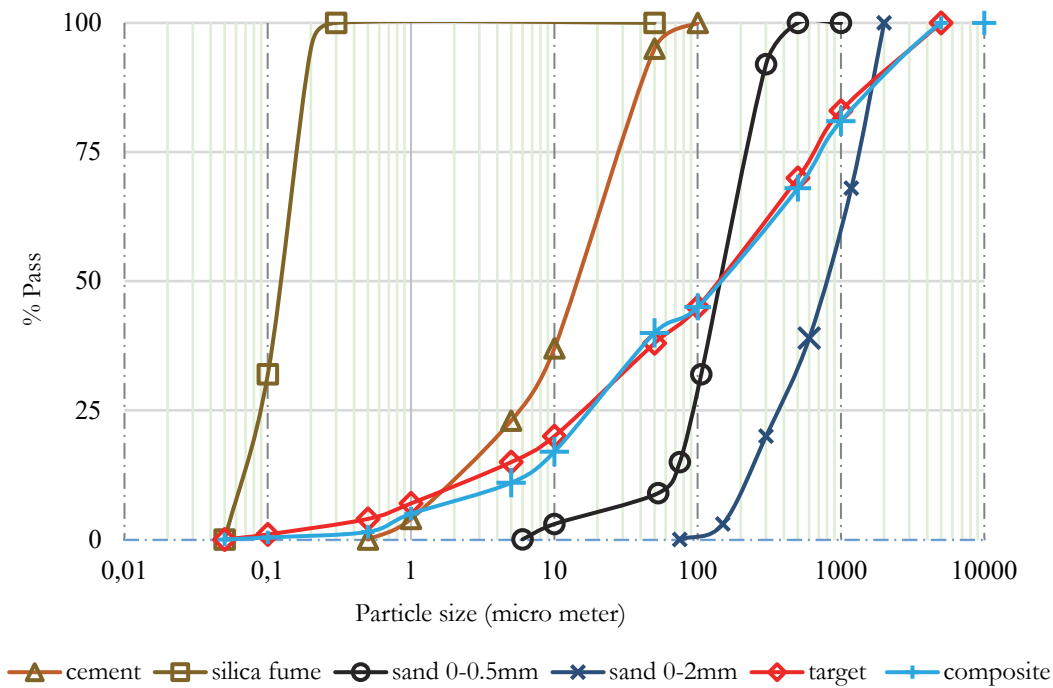


Figure 2: The grading curves of the used materials and the target and final composition curve.

Cubic Compressive strength (F_{cu})	Mix ID
35	NC
105	UHPC
125	UHPFRC1
140	UHPFRC2

Table 2: Compressive strength after 28 days (MPa)

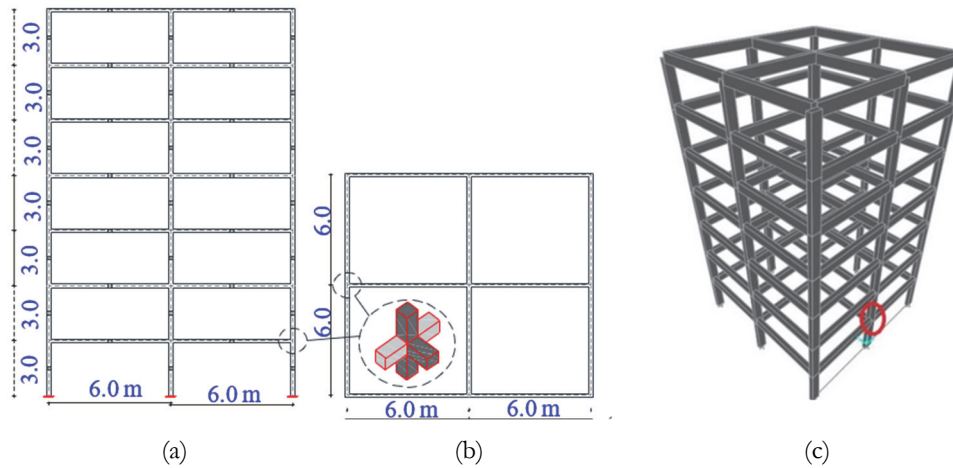


Figure 3: Structure details. a) 2D; b) Plan; c) sap2000 model.

Determining the dimensions of the samples and the most common differences among them

The samples were extracted from a (7storeyes-two bays) structure with a 3.0 m floor height and 6.0 m effective spans, as illustrated in Fig. 3. Using Sap2000 software [35], the building was analyzed. The structure was built in a zone with the following characteristics: medium soil (c) – seismic zone (3) – response spectrum curve type (1). F_y (yield stress of the steel) =360MPa, F_{cu} (Cubic Compressive strength of the concrete) =35MPa, finishing load=1.5kN/ m² . , and live load=2 kN/ m² . were used in the analysis. The building was computationally modeled under gravity and seismic loads under Egyptian Building Codes ECP No. 201 [36] to get the worst case for bending and shear forces for the BCJs utilized in this investigation. An exterior joint was selected to be designed with/without seismic design recommendations to determine cross-section dimensions and steel reinforcement details. The recommendations of the Egyptian code (ECP 203- 2018) [33] and ACI 352 R [37] were used to ensure that the chosen exterior joint fulfills the principle of a strong column-weak beam (The joint columns have sufficient ductility). The following condition must be met for the previous principle to be confirmed. The sum of the nominal flexural strengths of the column sections above and below the joint, calculated using the factored axial load that results in the minimum column-flexural strength, should not be less than 1.2 times the sum of the nominal flexural strengths of the beam sections at the joint. Although the beam and the column have the same cross-section, the samples fulfilled the recommendation of sufficient ductility for the joint columns because the columns contain a larger area of steel reinforcement, and the exterior joint contains two columns that work together and one beam only. The critical length of both column and beam was determined based on the recommendations of the Egyptian code [33]. The joint area was at the contra flexure points in the column and the beam to facilitate the representation of joint ends in the lab. To accommodate lab instruments, lengths, cross-sections, and steel reinforcement area were scaled to a (1/3) scale. The section dimensions for the column and beam in the tested joints were 130 mm X 230mm. The column length is 1.33m, and the length of the beam is 0.6m. Two 10 mm steel bars on the top and two 12mm on the bottom were used for beam reinforcing. There are 150 mm spacing of transverse reinforcements for beams and columns. For column reinforcement, four 12 mm steel bars were used. The steel reinforcement yield, ultimate stresses, and young’s modulus were 360 MPa, 520 MPa, and 200G Pa, respectively. The main features of this study are:

- a) Using different types of Concrete (NC, UHPC, and UHPFRC) on the behavior of beam-column joint.
- b) Steel fibers volume fraction (1% and 2%) of end-hooked steel fibers.
- c) Casting UHPFRC in the whole specimen or the critical joint zone only.
- d) Condensing stirrups at joint critical zone.
- e) Eliminating the stirrups from the joint zone.

Eight exterior beam-column joint samples were cast and tested. The details and differences between the samples are shown in Tab. 3. Two samples were poured with NC in the whole sample. The first sample was the control and consistent with the seismic design specifications, so the stirrups were condensed in the critical zone (spacing among stirrups in the critical zone was only 70 mm). The second sample (J1-NC) had normal transverse reinforcement details (spacing between the stirrups in sample 150 mm), as shown in Tab. 3. The next three samples (J1-UHPC, J1-UHPC1, and J1-UHPC2) were cast with UHPC, UHPFRC1, and UHPFRC2, respectively and have normal transverse reinforcement details as shown in Tab. 3. Another two samples, J1-UHPC-J and J1-UHPFRC1-J, were poured with UHPC and UHPFRC1, respectively, at the joint critical zone only, and the remaining part of the sample was poured with NC, and normal transverse reinforcement

details were used for the two samples (spacing 150 mm). The last sample was J2-UHPC2-J which used UHPFRC2 at the critical lengths and no stirrups in the joint zone. Fig. 4. shows the dimensions and steel reinforcement details.

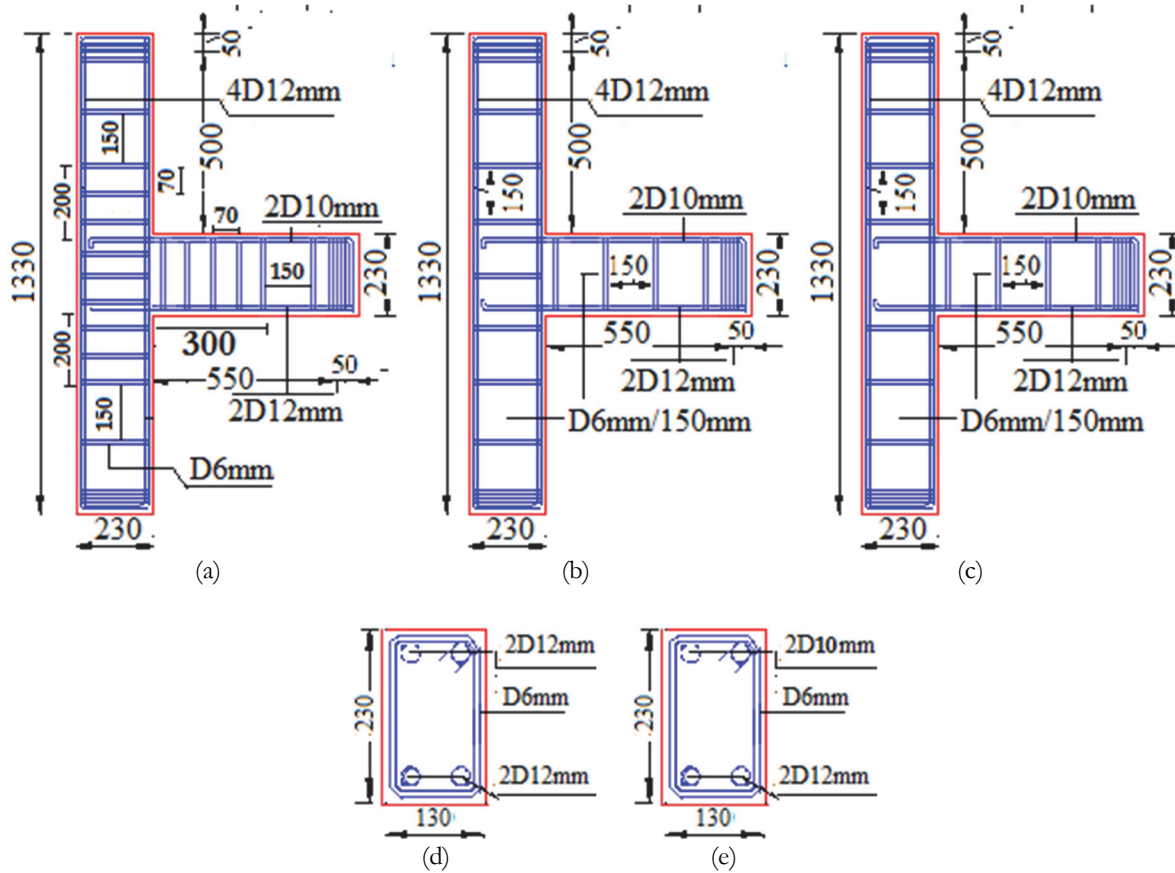


Figure 4: Details of joint reinforcements. a) Control connection (RFC), b) Stirrups at 150 mm (RF1), c) No stirrups at the joint core (RF2), d) column cross-section, e) beam cross-section.

Sample	The type of Concrete in the Joint	The type of Concrete in the rest of the sample	RF* details	Stirrups in the joint zone
Control	NC	NC	RFC	$\Phi 6 @ 60\text{mm}$
J1-NC	NC	NC	RF1	$\Phi 6 @ 150\text{mm}$
J1-UHPC	UHPC	UHPC	RF1	$\Phi 6 @ 150\text{mm}$
J1-UHPFC1	UHPFRC1	UHPFRC1	RF1	$\Phi 6 @ 150\text{mm}$
J1-UHPFC2	UHPFRC2	UHPFRC2	RF1	$\Phi 6 @ 150\text{mm}$
J1-UHPC-J	UHPC	NC	RF1	$\Phi 6 @ 150\text{mm}$
J1-UHPFC1-J	UHPFRC1	NC	RF1	$\Phi 6 @ 150\text{mm}$
J2-UHPFC2-J	UHPFRC2	NC	RF2	-

Note: *RF: Reinforcing details.

Table 3: Details of the exterior BCJ specimens.

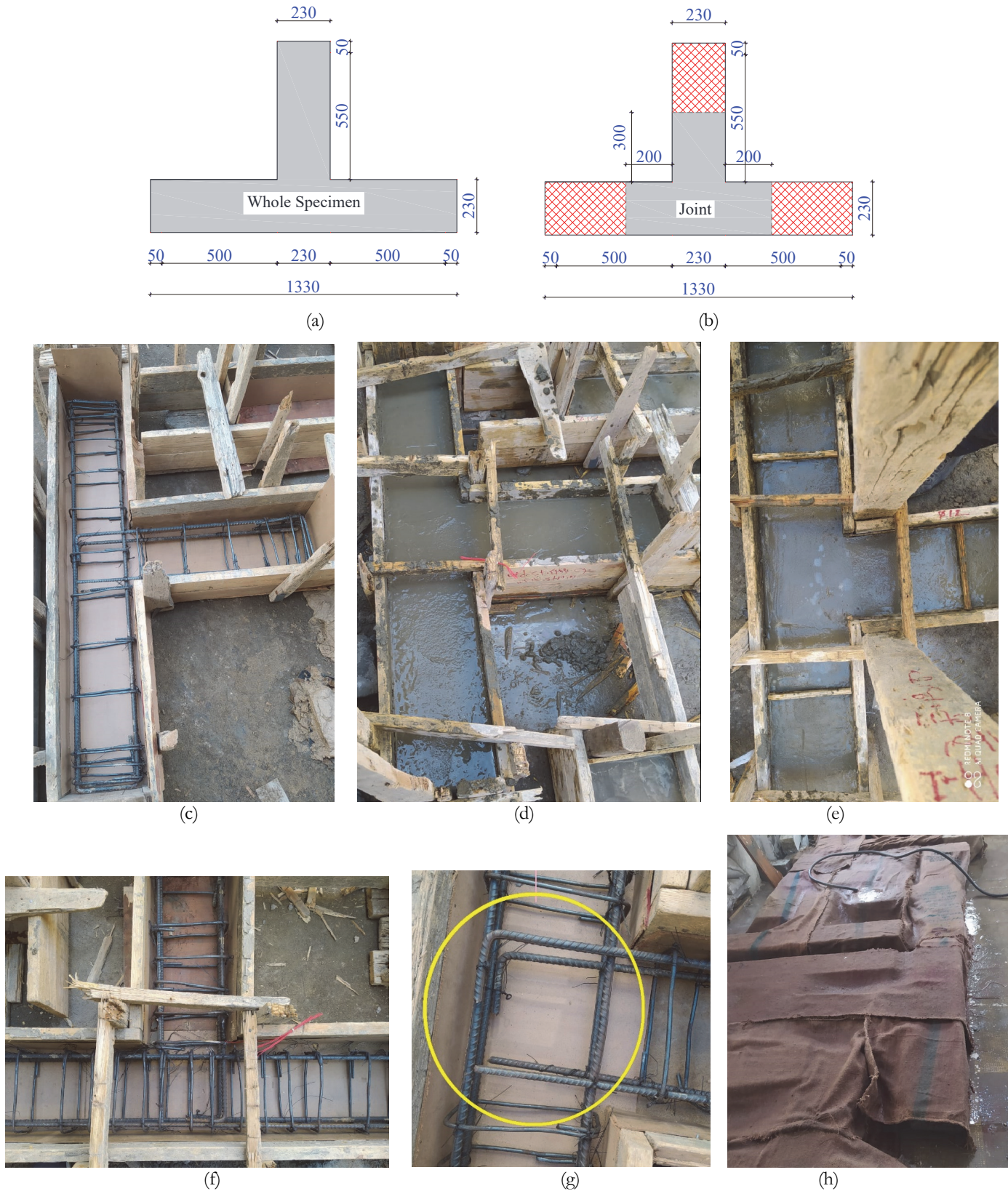


Figure 5: BCJs casting steps. a) BCJ dimensions; b) BCJ separated areas; c) Formwork and steel cages; d) Casting the whole formwork; e) Separation of the casting of the connection; f) condensing of stirrups in the critical lengths, g) sample without stirrups in the joint, h) Samples treatment.

Test setup and arrangement

The BCJs were tested under cyclic loading. The ends of the sample were supported to give the same bending diagram as the selected part of the joint in the actual structure. The two ends of the column are hinges supported using I beams and steel rods in the lab. The column of the sample is under constant load that conserves the stability of the sample. The end of the beam is free and under the test load, as shown in Fig. 6a-6b. For the testing procedure, two hydraulic jacks were used. The first was a 250kN hydraulic jack at the top of the column to apply axial load. The second was a movable hydraulic jack (capacity= 350kN) to apply repeated load at the beam end. Two load cells were used to measure the forces. A linear variable differential transformer (LVDT) was attached to the free end of the beam to measure the deflection, as shown in Fig. 6a-6b. A steel strain gauge was placed on the surface of the main reinforcement bars of the beam, and a concrete strain gauge was placed at the upper surface of the concrete of the beam. The load pattern used in this study is in one direction at the end of the beam. According to [38], the one-sided repeated loading pattern can simulate and describe earthquakes' inelastic requirements and behavior. The load pattern consists of repeated loading and unloading cycles (load returns to zero), as shown in Fig. 6c. The hydraulic jack applied the load at the beam's free end at a constant rate of 5 kN per minute. In the first cycle, the load is gradually increased from zero until reaching a value of 5kN at a constant rate of 5kN/minute, and then the load is gradually removed at the same rate until it reaches zero loads. In the following cycles, the loading pattern is carried out in the same manner as the previous one, with an increase in the value of the maximum load by 5 kN from the previous cycle. The maximum load values for successive cycles are (5, 10, 15, 20, etc.). The loading continues in the same previous pattern until the collapse of the sample occurs. The sample cannot bear the increase in the load imposed for the next cycle and when large cracks occur in the joint.

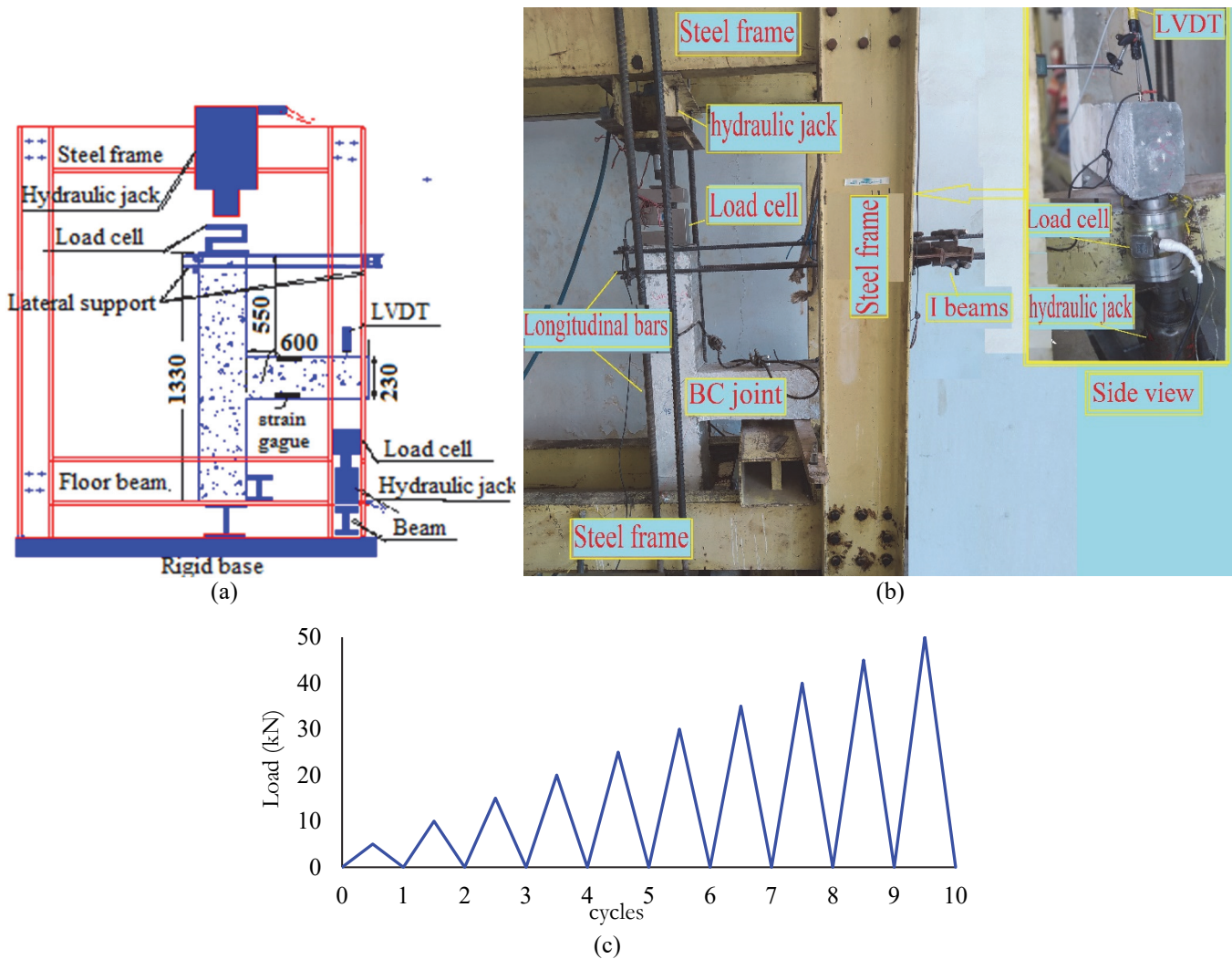


Figure 6: Test setup and applied load. a) Sample setup; b) Lab setup; c) Applied load.



EXPERIMENTAL RESULTS AND DISCUSSION

Failure modes and crack pattern

Tab. 4 shows all BCJs tested experimental findings, including peak load, deformations, first shear cracks, first flexure cracks, and failure modes. The initial flexural crack of beam-column specimens all occurred in the beam end near the column face during the crack stage, and the corresponding cracking loads were different for each case. The first shear crack appears at different cycles for all samples due to changes in sample properties. Fig. 7a displays the crack distribution on the control specimen. The first flexural cracks develop at the beam closest to the face of the column at 1.90% drift. Drift is the displacement at the end of the beam divided by the length of the beam measured from the center of the column to the free end of the beam $[(\Delta \text{ displacement}) / (\text{h length})]$. Most of the beam's minor flexural cracks are located close to the column's face, so the plastic hinge occurs in the beam. The crack size produced in the beam after the $d/2$ distance (beam depth/2) from the face of the column is moderately minor. Consequently, their contribution to energy absorption at the following load cycles is not regarded.

Sample ID	Ultimate load (kN)	η_{u1} (%)	Ultimate dis. (mm)	First flexure crack		First shear crack		Failure mode
				Load(kN)	Position	Load(kN)	Position	
Control	45	100	48	20	Beam-end	35	Beam-free end	FB
J1-NC	40	88.9	42	25	Beam end	30	Beam-end	FB-JF
J1-UHPC	45	100.0	53	20	Beam-end	30	Beam-end	SB-FB
J1-UHPFC1	58	128.9	61	25	Beam-end	30	Beam-end	FB
J1-UHPFC2	65	144.4	62	35	Beam-end	55	Beam-end	FB
J1-UHPC-J	45	100.0	52	25	Beam-end	30	Beam-end	FB
J1-UHPFC1-J	55	122.2	61	30	Beam-end	-	-	FB
J2-UHPFC2-J	65	144.4	74	35	Beam-end	-	-	FB.

Note: FB-JF = joint core failure with failure at the end of the beam; FB= flexure failure at the end of the beam; SB- FB= combination between shear failure and flexure failure of the beam; η_{u1} = (ultimate load for a sample /ultimate load for the control)

Table 4: Ultimate load, ultimate displacement, and mode failure.

The crack propagation of the (J1-NC) sample is presented in Fig. 7b. The earlier cracks in the (J1-NC) sample are formed identically to those in the control sample. Furthermore, transverse cracks in the joint core are developed in the 5.5 % drift, demonstrating that connection failure is near. The density of flexural and diagonal cracks increased with increasing load cycles. The concrete in the joint degraded with a 6% drift, the longitudinal reinforcement emerged, and the joint was destroyed. Shear failure of the joint core was caused by the lack of column ties in the connection area.

As shown in Fig. 7c, the first flexural cracks develop at the beam closest to the face of the column at 2.0 % drift. As illustrated in Fig. 8, the external cyclic loading causes normal compressive and shear stresses on the joint core. From Mohr's circle, the joint core's diagonal tensile and compressive stresses emerge from these stresses. Corresponding to principal stresses, the enhanced compressive and tensile strength of UHPC material in the specimen (J1-UHPC) will eliminate joint core degradation and shear failure.

In specimens containing steel fibers 1% and 2% (J1-UHPFC1 and J1-UHPFC2), a reasonable distribution of fibers improves the crack pattern (lengths and widths), limits crack opening and propagation, and controls lateral strain and material confinement, as shown in Fig. 7d,7e. Self-confinement of UHPFRC reduces the influence of shear reinforcement spacing in confinement, enhances the adhesion between reinforcement and concrete, and controls the reinforcement sliding in large drift ratios. The crack pattern of the sample (J1-UHPC-J) is similar to the crack pattern of (J1-UHPC), as shown in Fig. 7f. The (J2-UHPFC2-J) specimen has the same bearing capacity and ductility behavior as specimens with ties in the joint area. The joint core remained undamaged until the end of the experimental test. The crack pattern of (J1-UHPFC1-J) and (J2-UHPFC2-J) is similar, although the difference in load-carrying capacity between them, as shown in Fig. 7g,7h. Therefore, UHPFC material can use without transverse reinforcement in the BCJs. The specimen (J2-UHPFC-J) without shear links in the joint core is suggested as the ideal design owing to the intrinsic confinement of UHPFC materials, ease of construction, and low cost. The pattern of repeated loading in one direction made the places and directions of bending and shear cracks similar in all samples, but the cracks' lengths and widths depended on each sample's characteristics. As a result of not reversing the load in the other direction, new cracks do not form perpendicular to the previously formed cracks, but an expansion of the old cracks and an increase in length occurs during the loading cycles. The failure mode depends on the differences between the samples because they are subjected to the same loading pattern.

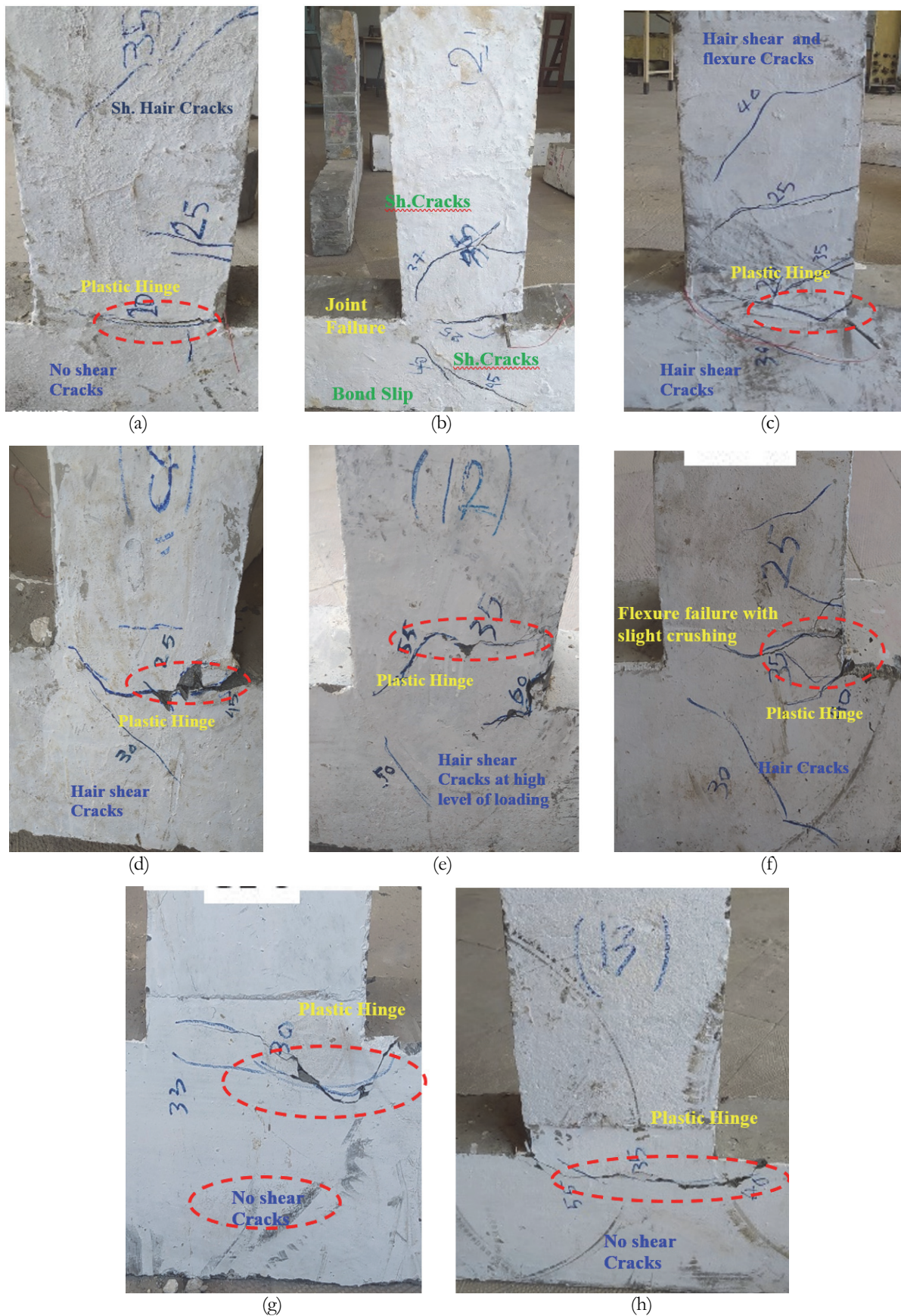


Figure 7: Cracking pattern and failure mode. a) Control; b) J1-NC; c) J1-UHPC; d) J1-UHPFC1; e) J1-UHPFC2; f) J1-UHPC-J; g) J1-UHPFC1-J; h) J2-UHPFC2-J.

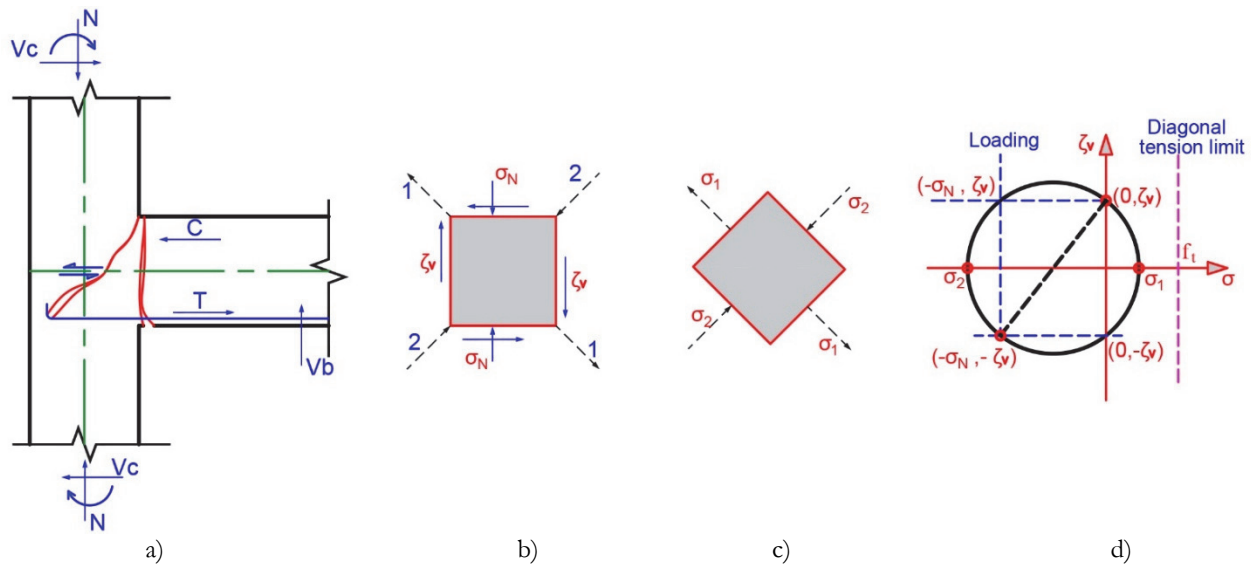


Figure 8: The principal stresses Mohr's circle. a) Subjected loading; b) Core stresses; c) Principal stresses; d) Mohr's circle stresses.

UHPFC samples with 1% steel fibers enhanced the behavior of the crack pattern compared with samples without steel fiber. Increasing steel fibers to 2% decreased the lengths, widths, and number of cracks. Ductile flexure failure was achieved by increasing steel fibers to 2%. Casting the whole sample with UHPFRC achieved very little improvement compared with sample casting at the joint zone only in the crack pattern. The presence of stirrups when the beam-column joint was cast with UHPFRC has little effect on its properties. Fiber bridging occurred in UHPFC samples due to the well spreading of fibers in the sample to reduce cracks width and stop the spreading of cracks in the sample. Using seismic design recommendations in the control sample could change the failure mode to ductile at the end of the beam and prevent the formation of cracks in the joint area. Similarly, the use of UHPFC with fibers ratios of 1 and 2% could achieve the same effect even with the use of reinforcement details without seismic recommendations and even with the use of UHPFC concrete in the joint area Only and also in the case of removing the stirrups from the joint area.

Hysteresis and envelope curves

Fig. 9 displays the hysteresis response of all tested BCJs. In the first cycles of the hysteresis curves, loading and unloading (removal) are parallel and close together. The displacement at the end of the unloading step was zero until the yield deformations. After that, the hysteric curve referred to the sample deformation with an increase in load (yield). The case returned to a small displacement through the unloading, and the next cycles started increasing the end deflection gradually. In the control sample, which satisfies the requirements of design codes, the confinement in the joint zone was improved, as shown in Fig. 9a. Consequently, the beam reinforcement did not slide prematurely, the specimen's behavior was ductile, and no substantial strength loss was noted until the test completion because of the condensation of the ties in the joint area. The sample (J1-NC) shows significant strength and stiffness degradation by load increase compared to the control sample, as shown in Fig. 9b, because the horizontal ties in the joint zone did not fulfill the requirements of seismic details; consequently, Shear cracks in the initial loading steps of the (J1-NC) specimen cause early slipping off the beam reinforcement and concrete degradation in the joint core; therefore, shear failure occurs.

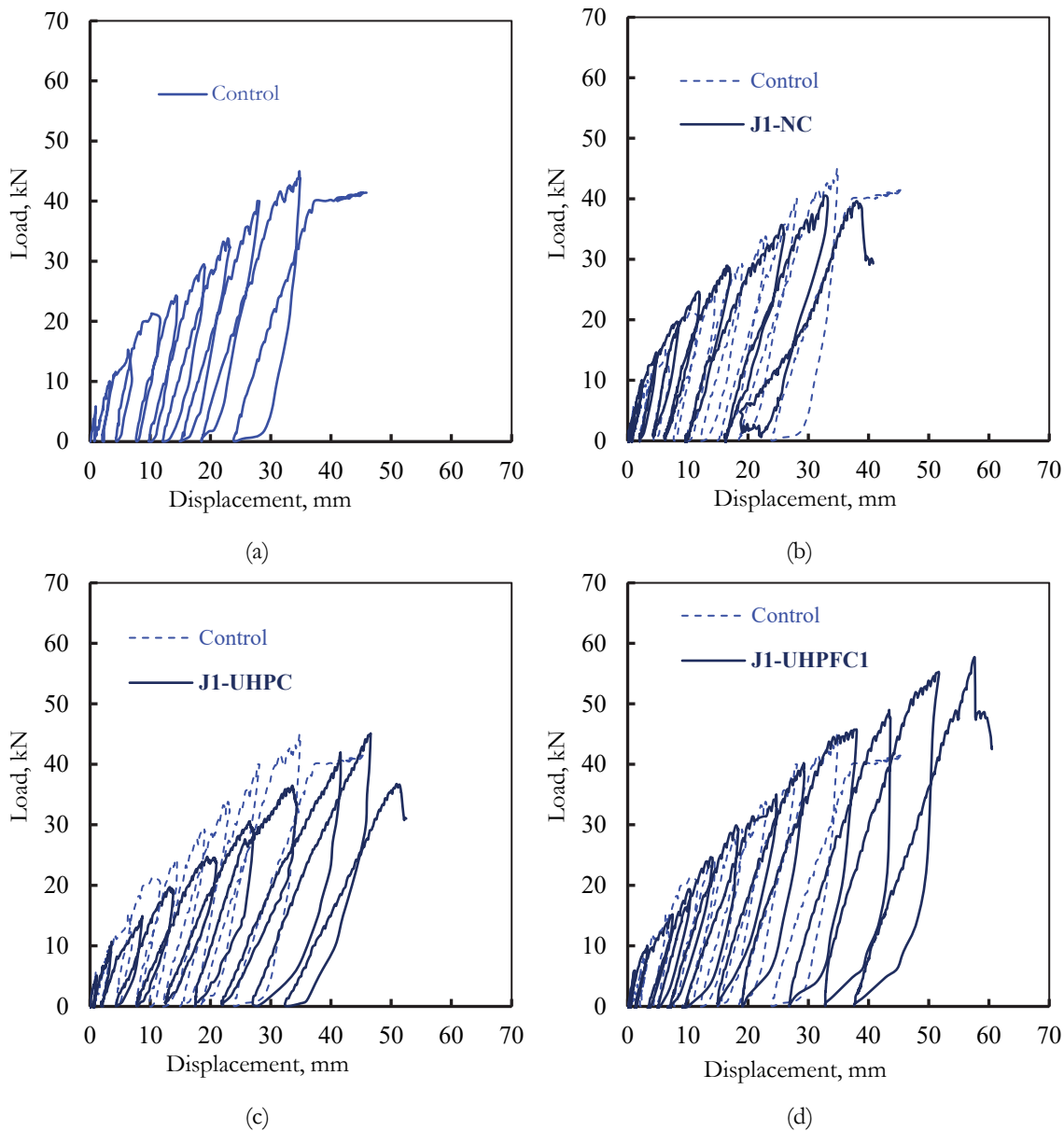
UHPC materials have strain-softening properties in tensile behavior because there are no coarse particles and homogeneous distribution of fine particles. Consequently, the (J1-UHPC) specimen significantly increases bearing capacity and the ultimate displacement compared to the control sample, as shown in Fig. 9c.

Using UHPFC with 1 and 2% steel fiber in the whole sample (J1-UHPFC1 and J1-UHPFC2) enhances maximum load and loop generation without any obvious decrease in stiffness and strength, as shown in Fig. 9d,e. It prevents the formation and propagation of cracks compared to the control sample. Also, there is no shear damage in the joint core, no slippage of the beam reinforcement, and inelastic behavior of the plastic hinge in the beam on the face of the column. This positive change could be attributed to steel bridging, which improves the bond strength of embedded reinforcing bars and UHPFC. Although UHPFC is used in the joint region only in samples (J1-UHPC-J), (J1-UHPFC1-J), and (J2-UHPFC2-J), the hysteresis curves are better than the control sample. (J1-UHPC-J) could reach ultimate displacement more than the control sample, as shown in Fig. 9f. (J1-UHPC-J) and (J1-UHPFC1-J) achieved ultimate displacement and load-carrying capacity

more than the control sample without any decrease in strength, as shown in Fig. 9g,9h. (J1-UHPFC1-J) was better than (J1-UHPC-J) in the hysteresis behavior due to using steel fiber in the mix.

The envelope curve is obtained by connecting the maximum points between the two branches of loading and unloading in successive cycles, as shown in Fig. (10). The envelope curve assures the improvement occurred for UHPFC samples through increasing ultimate load and increasing deflection. UHPFC samples are above other samples in the envelope curve.

UHPFC samples with 1% steel fibers (J1-UHPFC1, J1-UHPFC1-J) enhanced the behavior in load-carrying capacity more than samples without steel fiber (J1-UHPC, J1-UHPC-J) with (28.8,22.2%) and more than the control sample with the same previous proportions. Increasing steel fibers to 2% (J1-UHPFC2, J2-UHPFC2-J) increased load-carrying capacity by (44.4, and 62.5%) more than UHPC without steel fiber, control sample, and J1-NC, respectively. Casting the whole sample with UHPFC achieved little improvement compared with sample casting at the joint zone only in the crack pattern. The presence of stirrups when the beam-column joint is cast with UHPFC has little effect on its properties, so the specimen (J2-UHPFC2) without shear links in the joint core behaves similarly to the specimen (J1-UHPFC2).



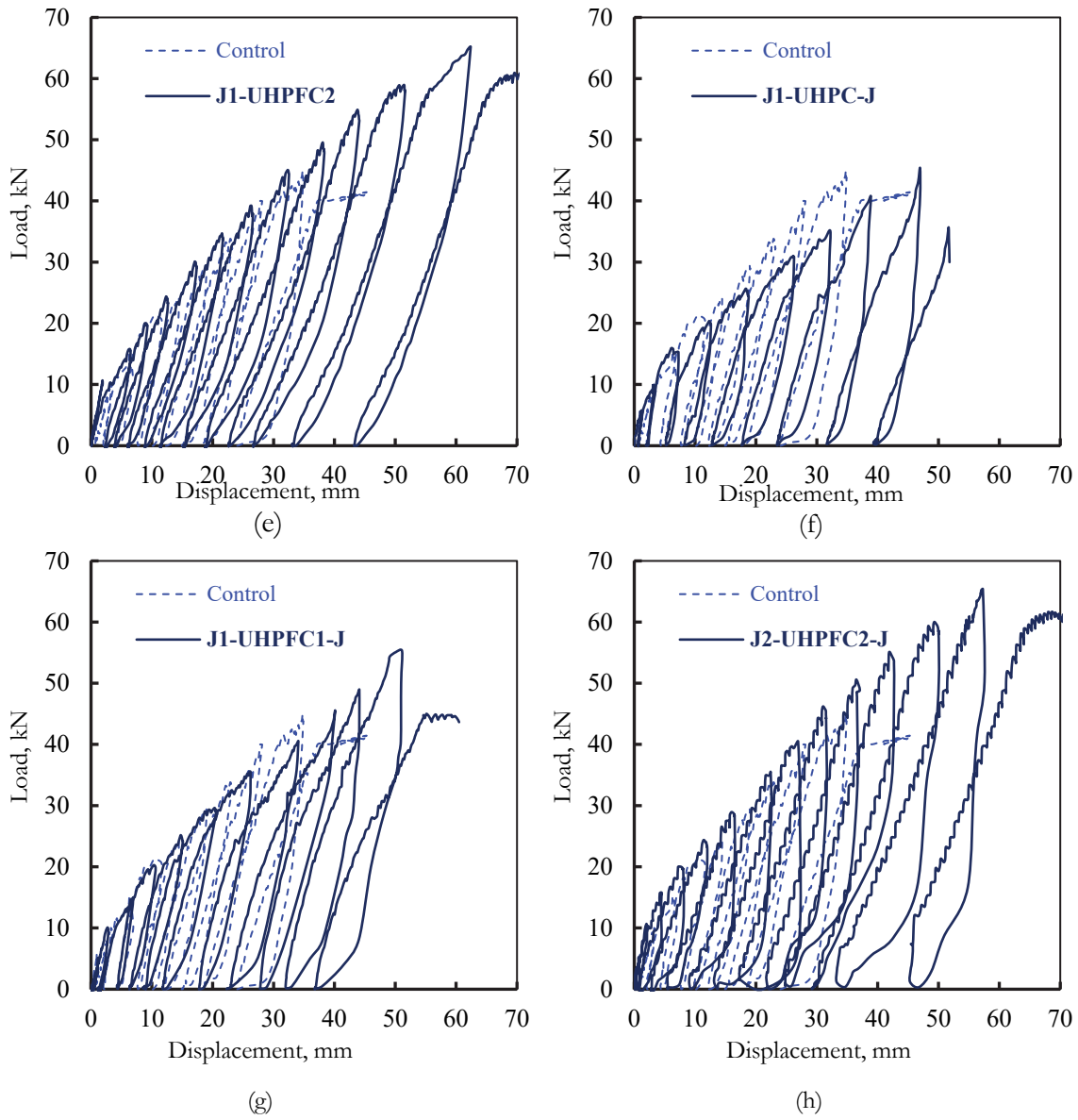


Figure 9: Hysteresis curves. a) Control; b) J1-NC; c) J1-UHPC; d) J1-UHPFC1; e) J1-UHPFC2; f) J1-UHPC-J; g) J1-UHPFC1-J; h) J2-UHPFC2-J

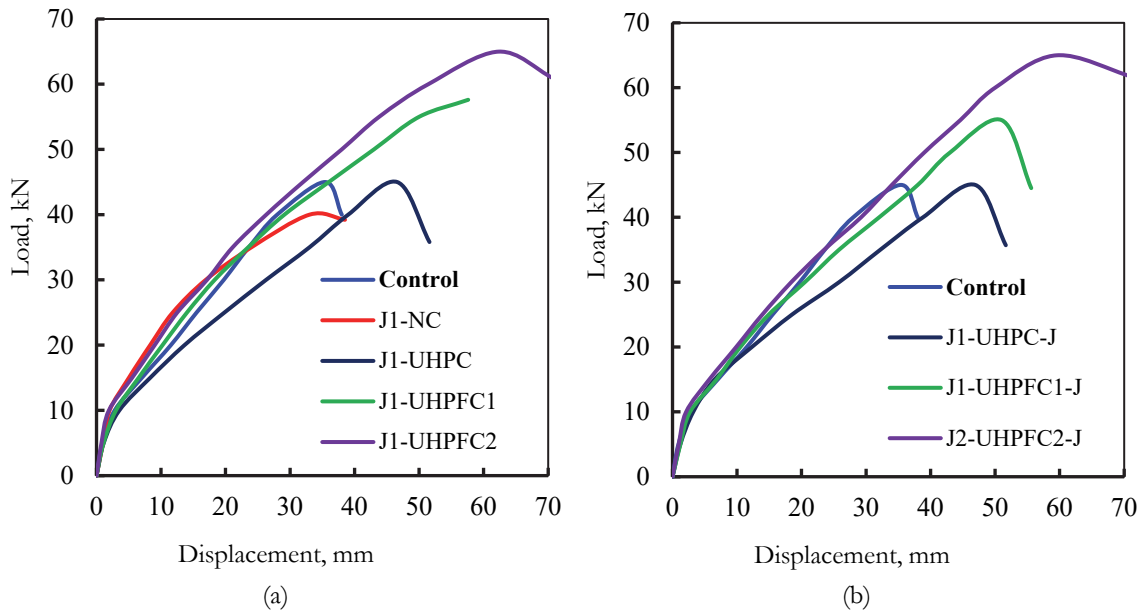


Figure 10: Envelope curve for all samples. a) The same material in the whole sample; b) Different materials in the sample.

Energy dissipation

The dissipated energy is the work absorbed by the structure to form cracks, displacements, and plastic hinges in the element. It is a part of the external energy acting on the structure. The total dissipated energy is the area under the envelope curve [39]. The dissipated energy of one cycle is the enclosed area between the loading curve and the unloading curve for the cycle, as in Fig. (11-a) through the following equations:

$$\text{Energy dissipation} = A_{\text{net}} = A_1 - A_2 \quad (\text{kN}\cdot\text{mm}) \quad (2)$$

$$A_1 = h/2 \cdot (2h_1 + 2h_2 + b) \quad (\text{kN}\cdot\text{mm}) \quad (3)$$

$$A_2 = h/2 \cdot (2h_3 + 2h_4 + b) \quad (\text{kN}\cdot\text{mm}) \quad (4)$$

where: A_1 and A_2 ; the area under the loading and unloading curve calculated by the trapezoidal rule; h , h_1 , h_2 , h_3 , h_4 , and b are illustrated in Fig. (11-b,c).

The cumulative dissipated energy at a cycle can be calculated by adding the dissipated energy during that cycle to the energy dissipated during the previous cycles, as shown in Fig. 12.

The external energy on structures is dissipated by the formation of cracks, friction between surfaces of the cracks, opening and closing of the formed cracks, and expansion of cracks' lengths and widths. Using steel fibers causes bridges between the cracks, participating in dissipating energy. In the first part of the cumulative energy dissipation curve, as shown in Fig. (12-b), the curves are parallel and very close because the energy dissipation in the first cycles is close between samples, as normal concrete and UHPFC have similar elastic modulus. In the last part of the cumulative dissipated energy curve, the divergence between the curves of the samples is observed because of the difference in cumulative energy dissipation values between the samples. The energy dissipated by a cycle of the last cycles is higher than that of the first cycle because of the high dissipated energy by spreading cracks and high displacement. Total energy dissipation for a sample is the sum of energy dissipated by every cycle for that sample. UHPFC specimens dissipate more energy than normal concrete because the fibers cause bridging between cracks and inhibit the cracks from spreading or opening.

UHPFC samples with 1% steel fibers (J1-UHPFC1, J1-UHPFC1-J) are higher in total energy dissipation than UHPC samples without fibers (J1-UHPC, J1-UHPC-J) with (38.6 and 38.1%) and (41.4 and 40.8%) respectively and higher than control sample (seismic dls) with (46.5 and 47.1%) and higher than (J1-NC) with (28 and 25%). UHPFC samples with 2% steel fibers (J1-UHPFC2, J2-UHPFC2-J) were higher in total energy dissipation than UHPC samples without fiber (J1-UHPC, J1-UHPC-J) with (50.5 and 69.2%) and (80.1 and 72.6%) respectively. Samples poured with UHPFC in the whole sample (J1-UHPC, J1-UHPFC1, J1-UHPFC2) were slightly more in total energy dissipation than those poured with UHPFC in the

joint zone only (J1-UHPC-J, J1-UHPFC1-J, J2-UHPFC2-J) in the different steel fiber ratios used in this study with an increase (2, 0.7, and 4.3%). The UHPFC sample (J1-UHPFC2) was slightly more than the UHPFC sample without srrops (J2-UHPFC2-J) in total energy dissipation with an increase (of 4.3%).

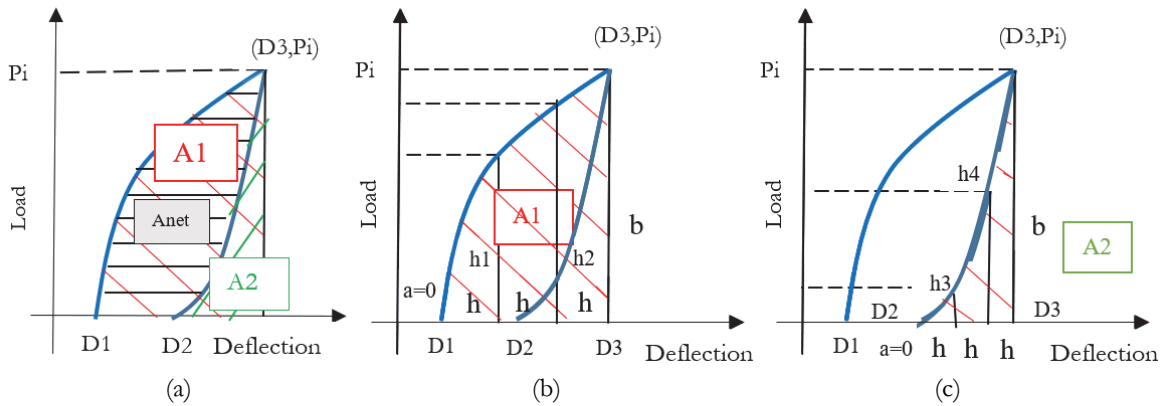


Figure 11: Energy dissipation calculation per cycle. a) Calculation of Anet, b) Calculation of A1, c) Calculation of A2.

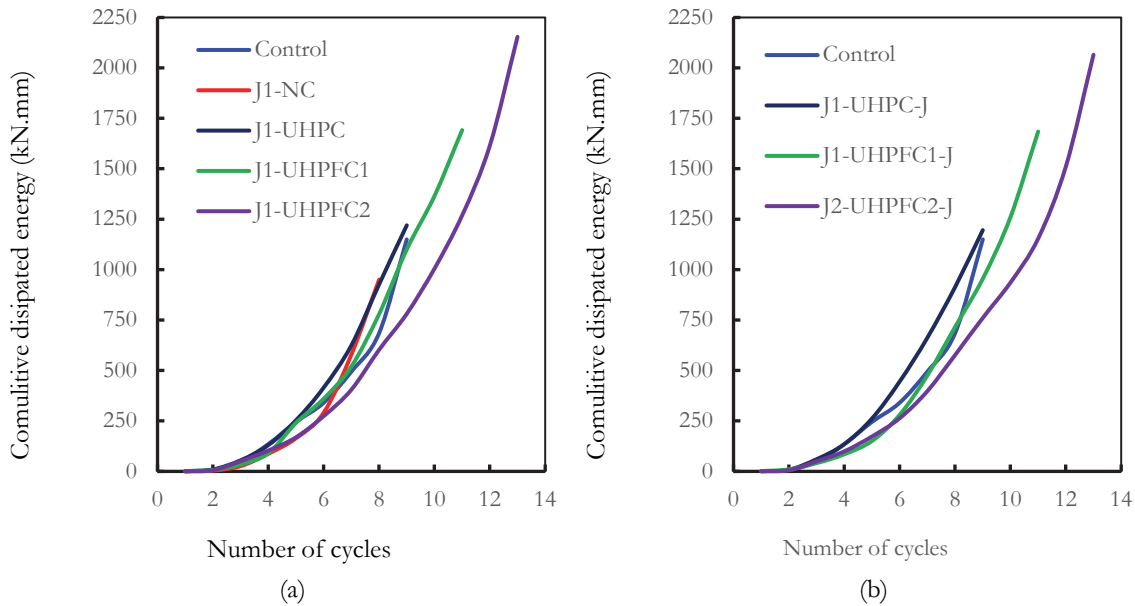


Figure 12: Cumulative energy dissipation per cycle. a) The same material in all sample; b) Different materials in the critical zone.

Stiffness degradation

The stiffness is the force needed to make a unit displacement at the end of the beam for a sample beam-column joint [39]. The slope of the secant line of a cycle's curve is used to measure its stiffness, as shown in Fig. 13 and the following equation:

$$K = P/D \text{ (kN/mm)} \tag{5}$$

Note; K= secant stiffness; P= max. load of the cycle; D is the displacement at the maximum Load minus displacement at the beginning of the loading curve. (Displacement through the cycle)

In the first cycles, the stiffness is higher than in the following cycles because samples are without effective cracks in the first. In the following cycles, cracks generate in the sample, so the sample becomes weak, and the bond between concrete and steel decreases (a small load can make a large displacement). Stiffness at the last cycles is lower than the stiffness at the first cycles. The divergence between the stiffness curves of the first cycles is observed due to the differences in the initial stiffness of samples. The stiffness deterioration during successive loading cycles on the sample is shown in Fig. 14. As displacement increases, the stiffness decreases. Yielding of joint core, nonlinear deformation of the concrete, loss of concrete covering, and reinforcing slippage all contribute to the samples' decreased stiffness. UHPFC samples with 1% steel fibers (J1-UHPFC1, J1-UHPFC1-J) are higher in initial stiffness than UHPC samples without fibers (J1-UHPC, J1-UHPC-J) with

(10 and 7.5%) and (12.5 and 9.6%) respectively and higher than control sample (seismic details) with (4.46 and 1.78%) and higher than (J1-NC) with (17 and 14%). UHPFC samples with 2% steel fibers (J1-UHPFC2, J2-UHPFC2-J) were higher in initial stiffness than UHPC samples without fiber (J1-UHPC, J1-UHPC-J) with (19.8 and 18.3%) and (22.1 and 20.5%) respectively and higher than control sample (seismic details) with (13.3 and 11.9 %). Samples poured with UHPFC in the whole sample (J1-UHPC, J1-UHPFC1, J1-UHPFC2) were slightly more in initial stiffness than those poured with UHPFC in the joint zone only (J1-UHPC-J, J1-UHPFC1-J, J2-UHPFC2-J) in the different steel fiber ratios used in this study with an increase (1.9, 2.6, and 1.2%). The UHPFC sample (J1-UHPFC2) was slightly more than the UHPFC sample without stirrups (J2-UHPFC2-J) in initial stiffness with an increase (1.2%).

Fiber bridging delayed the appearance and spreading of cracks in the sample, so the initial stiffness of UHPFC samples is increased more than other samples. The stiffness curve in initial cycles is steep, so stiffness deterioration is rapid, but the stiffness curve is a little gradient in the rest samples, so deterioration is gradual. In the last part of the stiffness curve, convergence is observed between curves because of the closeness of stiffness between samples. The stiffness deteriorated due to the spreading of cracks and failure.

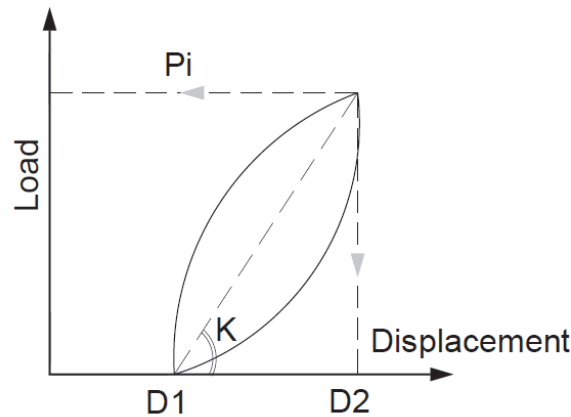


Figure 13: Cyclic stiffness calculation.

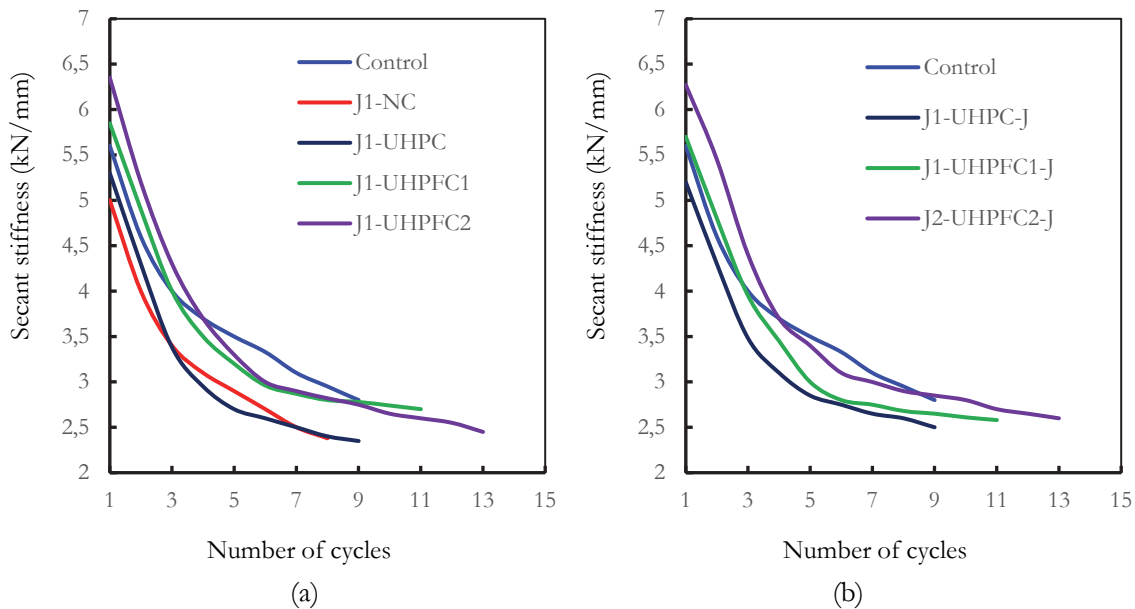


Figure 14: Stiffness degradation of all samples. a) The same material in all sample; b) Different materials in the critical

Ductility factor

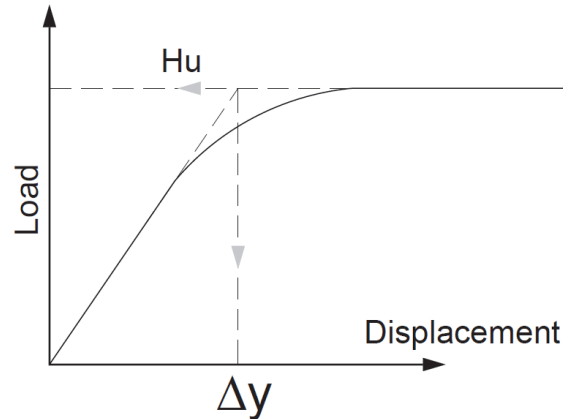
Any structure needs to behave in a ductile manner when exposed to loads to give warnings before the collapse and the opportunity to save lives and properties. Ductility is the ability of the structure to undergo large deformations in the inelastic



range without a significant reduction in strength. It is the ratio between the ultimate deflection of the sample and the yield deflection [40], as shown in Eqn. (6). Envelope curves that were plotted in Fig. 10 were used in the calculation.

$$\mu = \Delta_u / \Delta_y \quad [40] \tag{6}$$

Note; Δ_u = maximum deflection for the sample; Δ_y = yield deflection calculated from Fig. (15) depends on an equivalent elastic-plastic system with the same elastic stiffness and ultimate load as the real system [40].



15: Calculation of yield deflection using envelope curves.

Tab. 5 shows ductility factor values for all samples. UHPFC samples with 1% steel fibers (J1-UHPFC1, J1-UHPFC1-J) are higher in ductility factor than UHPC samples without fibers (J1-UHPC, J1-UHPC-J) with (18.3 and 16.1%) and (19.5 and 17.3%) respectively and higher than control sample (seismic details) with (26.6 and 24.2%) and higher than (J1-NC) with (41.4 and 38.7%). UHPFC samples with 2% steel fibers (J1-UHPFC2, J2-UHPFC2-J) were higher in ductility factor than UHPC samples without fiber (J1-UHPC, J1-UHPC-J) with (35 and 31.2%) and (36.4 and 32.5%) respectively and higher than control sample (seismic details) with (44.8 and 40.7%). Samples poured with UHPFC in the whole sample (J1-UHPC, J1-UHPFC1, J1-UHPFC2) were slightly more in ductility factor than those poured with UHPFC in the joint zone only (J1-UHPC-J, J1-UHPFC1-J, J2-UHPFC2-J) in the different steel fiber ratios used in this study with an increase (1, 1.9, and 2.9%). The UHPFC sample (J1-UHPFC2) was slightly more than the UHPFC sample without stirrups (J2-UHPFC2-J) in initial stiffness with an increase (2.9%). (J2-UHPFC2) without shear links in the joint core behaves similarly to the specimen (J1-UHPFC2), which has stirrups in the joint zone but does not meet the seismic detailing and performs better than the control sample. The cause for this is better tensile and shear strength, UHPFC bonding with embedded reinforcements, reinforcement sliding avoidance, joint zone damage prevention, and the plastic hinges in the beam.

Sample ID	Ductility factor	$\eta_{\mu 2}$ (%)
Control	4.58	100
J1-NC	4.1	89.5
J1-UHPC	4.9	107.0
J1-UHPFC1	5.8	126.6
J1-UHPFC2	6.62	144.5
J1-UHPC-J	4.85	105.9
J1-UHPFC1-J	5.69	124.2
J2-UHPFC2-J	6.43	140.4

Table 5: ductility factor of all samples.



CONCLUSIONS

This study studied the effect of (UHPFC) with end-hooked steel fiber of different volume fractions (0, 1, and 2%) on joints under repeated loads. UHPFC was poured at the whole sample in some samples and the joint region only in others. Eliminating stirrups of (UHPFC2) joint was studied as a solution for congestion of steel reinforcement. A comparison between the effect of (UHPFC) samples (UHPC, UHPFC with 1% steel fiber, and UHPFC with 2% steel fiber) and normal concrete samples with seismic design recommendations and without was carried out. Eight exterior (BCJ) samples were tested under repeated loading to reveal failure modes. Crack pattern, hysteresis curve, envelope curve, ductility factor, stiffness degradation, and energy dissipation were calculated. The following conclusions are derived obtained from the experimental study results:

1. The flexure failure and the plastic hinge occurred at the beam in all UHPFRC samples and the control sample because UHPFC could strengthen the joint zone well against shear failure. The control sample satisfied the seismic reinforcing specifications. In a normal concrete sample without seismic reinforcing specifications, shear failure occurred in the joint zone.
2. UHPFC samples with 2% steel fibers were the best in the crack pattern then UHPFC samples with 1% were better than the other samples by decreasing the cracks' number, lengths, and widths, increasing load-carrying capacity, and preventing the formation and propagation of cracks. Steel fiber bridging, which enhances the adhesion capacity of embedded reinforcing bars and UHPFRC materials, might be responsible for this favorable shift.
3. UHPFC with 1% and 2% steel fiber increased load-carrying capacity by (28.8 and 22.2%) and (44.4) compared to UHPC without fiber, respectively, and increased initial stiffness with proportions ranging (from 7.5 to 12.5%) and (from 18.3 to 22.1%) compared to UHPC without fiber respectively, ductility factor with (16.1 to 19.5%) and (31.2 to 36.6) compared to UHPC without fiber respectively and dissipated energy with (38.1 to 41.4%) and (69.1 to 80.1) compared to UHPC without fiber respectively. Increased fiber ratio improved the previous properties. UHPC samples without steel fiber improved the previous properties more than the normal concrete sample (J1-NC).
4. The samples poured with UHPFC at the whole sample were extremely identical to the samples poured with UHPFC at the joint only in the crack pattern and load-carrying capacity but slightly more in initial stiffness with an increase (1.9, 2.6, and 1.2%) in the different steel fiber ratios and total energy dissipation with increase (2, 0.7 and 4.3%) for UHPFC samples and ductility factor with increase (1, 1.9 and 2.9%) in the different steel fiber ratios (0,1, and 2%). Limited improvement occurred when pouring the whole sample, so pouring the joint only, which is an economical solution, can be considered.
5. Eliminating stirrups from (J2-UHPFC2-J) didn't affect the behavior of the joint. (J1-UHPFC2) sample with minimum stirrups in the joint was extremely identical to the UHPFC sample without stirrups in the crack pattern, load-carrying capacity but slightly more in initial stiffness with increase (1.2%) and total energy dissipation with increase (4.3%) and ductility factor with increase (2.9%). The specimen from UHPFC without shear reinforcement in the joint zone is suggested as the ideal design owing to the intrinsic confinement of UHPFC materials, ease of construction, and low cost.
6. The testing results of UHPFC specimens show that this material can ensure excellent joint behavior even pouring UHPFC in the joint only or without using shear ties in the joint core. It is possible to achieve much more desired behavior than concrete joints that fulfill the criteria of seismic reinforcing details. Better tensile and shear strength, UHPFC bonding with embedded reinforcements, reinforcement slide avoidance, joint zone damage prevention, and the creation of plastic hinges in the beam are all factors contributing to this.

In future studies, the effect of using percentages of fibers not mentioned in the research, such as 0.5% and 1.5%, can be studied. The effect of the repeated load, which is reversed in the other direction, on the behavior of the samples can be studied. The effect of deleting the stirrups from the critical joint zone can be studied on the different ratios of the steel fibers. Studying the possibility of achieving the same improvement effect for the samples in which longitudinal beam bars were anchored in the joint using UHPFRC.

The author declares that they have no known competing financial interests or personal relationships that could have appeared to influence the work reported in this paper.

The authors extend their thanks to the journal and the reviewers for their assistance in improving the document level and to the Faculty of Engineering, Zagazig University's laboratory, for their cooperation in pouring samples and conducting tests.



REFERENCES

- [1] Murad, Y.Z. (2022). Retrofitting heat-damaged non-ductile RC beam-to-column joints subjected to cyclic and axial loading with FRCM composites. *Journal of Building Engineering*, 48, p.103952. DOI: 10.1016/j.job.2021.103952.
- [2] Rahmani, A. Y., Boukhalkhal, S. H. and Badaoui, M. (2022). Effect of beam-column joints flexibility on the seismic response of setback RC buildings designed according to the Algerian seismic code, *Frattura ed Integrità Strutturale*, 16(61), pp. 394–409. DOI: 10.3221/IGF-ESIS.61.26.
- [3] Ravikumar, S. and Kothandaraman, S. (2022). Experimental Study on Performance of Ductile and Non-ductile Reinforced Concrete Exterior Beam-column Joint. *International Journal of Engineering*, 35(7), pp.1237-1245. DOI: 10.14445/22315381/IJETT-V70I3P210.
- [4] Paulay, T. and Scarpas, A. (1981). The behaviour of exterior beam-column joints. *Bulletin of the New Zealand Society for Earthquake Engineering*, 14(3), pp.131-144.
- [5] Borujerdi, A.S., Mostofinejad, D. and Hwang, H.J. (2021). Cyclic loading test for shear-deficient reinforced concrete exterior beam-column joints with high-strength bars. *Engineering Structures*, 237, p.112140. DOI: 10.1016/j.engstruct.2021.112140.
- [6] Chitra, R. and Mohan, S.J. (2022). Reinforced concrete beam-column joint's ductility behavior. *Materials Today: Proceedings*, 51, pp.1069-1073. DOI: 10.1016/j.matpr.2021.07.096.
- [7] Chalioris, C.E., Favvata, M.J. and Karayannis, C.G. (2008). Reinforced concrete beam-column joints with crossed inclined bars under cyclic deformations. *Earthquake engineering & structural dynamics*, 37(6), pp.881-897. DOI: 10.1002/eqe.793.
- [8] Lee, J.Y., Kim, J.Y. and Oh, G.J. (2009). Strength deterioration of reinforced concrete beam-column joints subjected to cyclic loading. *Engineering Structures*, 31(9), pp.2070-2085. DOI: 10.1016/j.engstruct.2009.03.009.
- [9] Paulay, T. and Priestley, M.N. (1992). *Seismic design of reinforced concrete and masonry buildings*, 768. New York: Wiley.
- [10] Tran, M.T. (2016). Influence factors for the shear strength of exterior and interior reinforced concrete beam-column joints. *Procedia engineering*, 142, pp.63-70. DOI: 10.1016/j.proeng.2016.02.014.
- [11] Li, B. and Leong, C.L. (2015). Experimental and numerical investigations of the seismic behavior of high-strength concrete beam-column joints with column axial load. *Journal of Structural Engineering*, 141(9), p.04014220. DOI: 10.1061/(ASCE)ST.1943-541X.0001191.
- [12] Kaung, J.S. and Wong, H.F. (2011). Effectiveness of horizontal stirrups in joint core for exterior beam-column joints with nonseismic design. *Procedia Engineering*, 14, pp.3301-3307. DOI: 10.1016/j.proeng.2011.07.417.
- [13] Chun, S.C. and Shin, Y.S. (2014). Cyclic testing of exterior beam-column joints with varying joint aspect ratio. *ACI Structural Journal*, 111(3), p.693. DOI: 10.14359/51686730.
- [14] Kuang, J.S. and Wong, H.F. (2006). Effects of beam bar anchorage on beam-column joint behaviour. *Proceedings of the Institution of Civil Engineers-Structures and Buildings*, 159(2), pp.115-124. DOI: 10.1680/stbu.2006.159.2.115.
- [15] Pauletta, M., Di Marco, C., Frappa, G., Miani, M., Campione, G. and Russo, G. (2021). Seismic behavior of exterior RC beam-column joints without code-specified ties in the joint core. *Engineering Structures*, 228, p.111542. DOI: 10.1016/j.engstruct.2020.111542.
- [16] Cosgun, C., Turk, A.M., Mangir, A., Cosgun, T. and Kiyamaz, G. (2020). Experimental behaviour and failure of beam-column joints with plain bars, low-strength concrete and different anchorage details. *Engineering Failure Analysis*, 109, p.104247. DOI: 10.1016/j.engfailanal.2019.104247.
- [17] Xu, W. and Ronggui, L. (2015). Effect of steel reinforcement with different degree of corrosion on degeneration of mechanical performance of reinforced concrete frame joints, *Frattura ed Integrità Strutturale*, 10(35), pp. pages 481–491. DOI: 10.3221/IGF-ESIS.35.54.
- [18] Wille, K., Naaman, A.E. and Parra-Montesinos, G.J. (2011). Ultra-High Performance Concrete with Compressive Strength Exceeding 150 MPa (22 ksi): A Simpler Way. *ACI materials journal*, 108(1). DOI:10.14359/51664215.
- [19] Hung, C.C. and Chueh, C.Y. (2016). Cyclic behavior of UHPFRC flexural members reinforced with high-strength steel rebar. *Engineering Structures*, 122, pp.108-120. DOI: 10.1016/j.engstruct.2016.05.008.
- [20] Bermudez, M. and Hung, C.C. (2021). Shear Behavior of Steel Reinforced Ultra High Performance Concrete Members with Hybrid Fibers. In *EASEC16* (pp. 1645-1654). Springer, Singapore. DOI: 10.1007/978-981-15-8079-6_152.
- [21] Marchand, P., Baby, F., Khadour, A., Rivillon, P., Renaud, J.C., Baron, L., Genereux, G., Deveaud, J.P., Simon, A. and Toutlemonde, F. (2019). Response of UHPFRC columns submitted to combined axial and alternate flexural loads. *Journal of Structural Engineering*, 145(1), p.04018225. DOI: 10.1061/(ASCE)ST.1943-541X.0002209.



- [22] Emara, M., Mohamed, H.A., Rizk, M.S. and Hu, J.W. (2021). Behavior of ECC columns confined using steel wire mesh under axial loading. *Journal of Building Engineering*, 43, p.102809. DOI: 10.1016/j.job.2021.102809.
- [23] Hung, C.C. and Yen, C.H. (2021). Compressive behavior and strength model of reinforced UHPC short columns. *Journal of Building Engineering*, 35, p.102103. DOI: 10.1016/j.job.2020.102103.
- [24] Nguyen, D.L., Thai, D.K., Tran, N.T., Ngo, T.T. and Le, H.V. (2022). Confined compressive behaviors of high-performance fiber-reinforced concrete and conventional concrete with size effect. *Construction and Building Materials*, 336, p.127382. DOI: 10.1016/j.conbuildmat.2022.127382.
- [25] Yuan, F., Pan, J., Xu, Z. and Leung, C.K.Y. (2013). A comparison of engineered cementitious composites versus normal concrete in beam-column joints under reversed cyclic loading. *Materials and structures*, 46(1), pp.145-159. DOI: 10.1617/s11527-012-9890-6.
- [26] Al-Osta, M.A., Al-Khatib, A.M., Baluch, M.H., Azad, A.K. and Rahman, M.K. (2017). Performance of hybrid beam-column joint cast with high strength concrete. *Earthquakes and Structures*, 12(6), pp. 603-617. DOI: 10.12989/eas.2017.12.6.603.
- [27] Zheng, W., Wang, D. and Ju, Y. (2018). Performance of reinforced reactive powder concrete beam-column joints under cyclic loads. *Advances in Civil Engineering*. DOI: 10.1155/2018/3914815.
- [28] Said, SH and Razak, H.A. (2016). Structural behavior of RC engineered cementitious composite (ECC) exterior beam-column joints under reversed cyclic loading. *Construction and Building Materials*, 107, pp.226-234. DOI: 10.1016/j.conbuildmat.2016.01.001.
- [29] Suryanto, B., Tambusay, A., Suprobo, P., Bregoli, G. and Aitken, M.W. (2022). Seismic performance of exterior beam-column joints constructed with engineered cementitious composite: Comparison with ordinary and steel fibre reinforced concrete. *Engineering Structures*, 250, p.113377. DOI: 10.1016/j.engstruct.2021.113377
- [30] Sarmiento, P.A., Torres, B., Ruiz, D.M., Alvarado, Y.A., Gasch, I. and Machuca, A.F. (2019). Cyclic behavior of ultra-high performance fiber reinforced concrete beam-column joint. *Structural Concrete*, 20(1), pp.348-360. DOI: 10.1002/suco.201800025.
- [31] Ma, F., Deng, M. and Yang, Y. (2021). Experimental study on internal precast beam-column ultra-high-performance concrete connection and shear capacity of its joint. *Journal of Building Engineering*, 44, p.103204. DOI: 10.1016/j.job.2021.103204.
- [32] Abusafaqa, F.R., Samaaneh, M.A. and Dwaikat, M.B. (2022). Improving ductility behavior of sway-special exterior beam-column joint using ultra-high performance fiber-reinforced concrete. In *Structures (Vol. 36, pp. 979-996)*. Elsevier. DOI: 10.1016/j.istruc.2021.12.059.
- [33] ECP 203-2018. Egyptian Building Code for Structural Concrete Design and Construction. Ministry of Housing, Utilities and Urban Communities, Cairo (2018).
- [34] <http://www.sika.com>, (2022), Jan.10.
- [35] SAP, C., 2000. V-8.2. 3.(2002). *Integrated Finite Element Analysis and Design of Structures Basic Analysis Reference Manual*. Computer and Structures Inc., Berkeley. California.
- [36] ECP No. 201. Egyptian Code of Practice for Calculation of Loads and Forces in Structural and Masonry Works. Housing and Building National Research of Egypt, Giza, Egypt, (2012).
- [37] ACI Committee 352R-02, (2002). *Recommendations for the design of beam-column connections in monolithic reinforced concrete structures*. American Concrete Institute.
- [38] Maison, B.F. and Speicher, M.S. (2016). Loading protocols for ASCE 41 backbone curves. *Earthquake Spectra*, 32(4), pp.2513-2532. DOI: 10.1193/2F010816EQS007EP.
- [39] Nouri, A., Saghafi, M.H. and Golafshar, A. (2019). Evaluation of beam-column joints made of HPFRCC composites to reduce transverse reinforcements. *Engineering Structures*, 201, p.109826. DOI: 10.1016/j.engstruct.2019.109826.
- [40] Park, R., (1988). Ductility evaluation from laboratory and analytical testing. In *Proceedings of the 9th world conference on earthquake engineering*, 8, pp. 605-616. Tokyo-Kyoto Japan.